

# Enhancing electrochemical properties of $\text{TiO}_2$ nanotubes via engineered defect laden crystal structures

Hamad Malik <sup>a</sup>, Kai Barrera <sup>a</sup>, Swomitra Mohanty <sup>b</sup>, Krista Carlson <sup>a,\*</sup>

<sup>a</sup> Department of Materials Science and Engineering, University of Utah, Salt Lake City, UT, USA

<sup>b</sup> Department of Chemical Engineering, University of Utah, Salt Lake City, UT, USA



## ARTICLE INFO

### Article history:

Received 7 April 2020

Received in revised form 7 May 2020

Accepted 8 May 2020

Available online 15 May 2020

### Keywords:

Titanium dioxide

Nanostructures

Annealing

## ABSTRACT

This study identifies the dependence of electrochemical properties of titanium dioxide nanotubes (NTs) containing specific concentrations and locations of defects within the crystal structure. NTs, formed through electrochemical anodization, were annealed at 500°C in either oxygen ( $\text{O}_2$ -NTs) or 2% hydrogen with nitrogen balance (2% $\text{H}_2$ /N<sub>2</sub>-NTs). Examination of the NTs using scanning/transmission electron microscopy showed that the  $\text{O}_2$ -NTs were comprised of a mixed phase anatase–rutile, while the 2% $\text{H}_2$ /N<sub>2</sub>-NTs were primarily anatase with a defect laden disordered surface layer. Electrochemical impedance measurements showed enhanced electrochemical behavior of the 2% $\text{H}_2$ /N<sub>2</sub>-NTs compared to the  $\text{O}_2$ -NTs as a result of the defect-laden structure.

© 2020 Elsevier B.V. All rights reserved.

## 1. Introduction

Titanium dioxide nanotubes (NTs) are commonly studied for photoelectrocatalytic degradation of waterborne pollutants, pathogens [1], and for catalytic-based sensing of volatile organic compounds (VOCs) associated with environmental pollution or diseases. Titanium dioxide ( $\text{TiO}_2$ ) is a desirable semiconductor for aqueous photocatalysis because the width of its band gap and position of band edges are ideal for the photoinduced oxidation of to take place [1]. Electrochemical anodization is one of the easiest methods to form arrays of ordered amorphous NTs [2]. The random atomic arrangement of amorphous NTs displays weaker photoelectrocatalytic behavior than their crystalline counterparts. Annealing is typically performed to create specific crystal structures with enhanced charge transport and/or larger number of charge carriers [3]. Our group has reported on an electrocatalytic disinfection device that shows effective disinfection using NTs annealed in 2% hydrogen with nitrogen balance (2% $\text{H}_2$ /N<sub>2</sub>-NTs) [4,5]. Annealing in 2% $\text{H}_2$ /N<sub>2</sub> creates a heavily defect-laden structure within the NTs. This behavior is in contrast to NTs annealed in oxygen ( $\text{O}_2$ -NTs), which prefers phase transformation over defect formation resulting in a mixed anatase–rutile structure.

To our knowledge, no one has reported on engineering the crystalline NTs structure for enhanced electrochemical properties. In this study we have produced defect laden crystalline NTs

(2% $\text{H}_2$ /N<sub>2</sub>-NTs) and mixed oxide anatase–rutile NTs ( $\text{O}_2$ -NTs) to compare their electrochemical properties and determine the crystalline structure with enhanced electrochemical response.

This study reports on important factors leading to formation of different crystalline NTs structures, and the factors that causes these distinctive NTs structures to display significantly different electrochemical properties.

## 2. Materials and methods

NTs were synthesized using anodization procedure reported in the previous work [4,5]. Briefly, titanium foil (99.9%, Alfa Aesar) was cut into 2 cm by 2 cm strips and cleaned in 15% hydrochloric acid (HCl) and deionized water (DI). Cleaned foils were electropolished in 5% vinegar using an electrochemical cell with titanium foil as anode and platinum mesh as cathode. Foils were polished at 25 V for 1 min, and then cleaned using DI before anodizing in an ethylene glycol solution of 0.5 wt% ammonium fluoride and 3 wt % DI. Anodization was done at 30 V for 60 min. Half of the anodized foils were annealed using 2% $\text{H}_2$ /N<sub>2</sub>-NTs and the other half using  $\text{O}_2$ . Annealing was done in a controlled environment using a tube furnace. The furnace was set to reach 500°C in the 60 min and stay at 500°C for the 180 min before cooling back to room temperature in 60 min. The annealing temperature of 500°C was chosen because our previous studies have shown that the nanotubular morphology can be preserved within this temperature range also other researchers have shown that the highest number of defects are formed within this temperature range [6].

\* Corresponding author.

E-mail address: [krista.carlson@utah.edu](mailto:krista.carlson@utah.edu) (K. Carlson).

### 3. Characterization of nanotubes

Morphology of the NTs was examined using a field emission scanning electron microscope (FE-SEM, Hitachi, S-4800). Crystal phases were observed using x-ray diffractometer (RIGAKU Mini Flex 600) with  $\text{CuK}\alpha$  radiation ( $\lambda = 1.54$  Angstrom) between  $20 = 20 - 80^\circ$  at a rate of 0.025 /s and crystallite size was calculated from the peak widths using the Scherrer equation. Atomically resolved images of the NTs were generated using high-resolution transmission electron microscope (S/TEM, JEOL JEM-2800). Electrochemical testing was performed using potentiostat (Gamry Reference 600) and a standard 3 electrode cell with  $\text{Ag}/\text{AgCl}$  reference electrode, platinum gauge cathode and titanium foil anode in  $7 \times 10^{-4}$  M  $\text{K}_3[\text{Fe}(\text{CN})_6]$  in 1 M KCl electrolyte solution.

### 4. Results and discussion

Annealing in 2% $\text{H}_2$ - $\text{N}_2$  transforms the amorphous NTs to anatase with a crystallite size of 19 nm and a disordered surface layer due to hydrogenation (Fig. 1(a)). No anatase crystallites  $> 20$  nm were observed. This observation was in agreement with findings

previously reported in the literature, as crystallites  $> 20$  nm are thermodynamically unstable and act as a nucleation sites for stable rutile phases [7,8]. The disordered surface layer within these NTs is accredited to the chemical interaction of the NTs surface with 2% $\text{H}_2$ - $\text{N}_2$  gas. During annealing, elements in the  $\text{TiO}_2$  lattice interact with the 2% $\text{H}_2$ - $\text{N}_2$  gas producing surface defects including the oxygen vacancies ( $\text{V}_0$ ) and  $\text{Ti}^{3+}$  interstitials [9,10]. These defects are present as disorder at the surface of 2% $\text{H}_2$ - $\text{N}_2$ -NTs. The HRTEM image of 2% $\text{H}_2$ - $\text{N}_2$ -NTs show the interface between the crystalline structure (sharp lattice fringe) and a disordered surface layer separated by the dashed line (Fig. 1(a)).

The defect laden disorder surface layer provides trapping sites for the charge carriers, restricting their recombination upon excitation [3]. The formation of these defects result in n-type doping, optical bandgap narrowing and increase in the visible light absorption (Fig. 2(a)). Previous studies have shown that  $\text{Ti}^{3+}$  interstitials make shallow donor states below the conduction band [10] altering the bandgap of NTs from 3.2 eV to 2.7 eV (Fig. 2(b)).

In contrast to the 2% $\text{H}_2$ - $\text{N}_2$ -NTs, the  $\text{O}_2$ -NTs show higher phase transformation with amorphous  $\Rightarrow$  anatase  $\Rightarrow$  rutile phase changes. The  $\text{O}_2$ -NTs are composed of mixed phase anatase-rutile with approximately 50% of each anatase and rutile phase. The

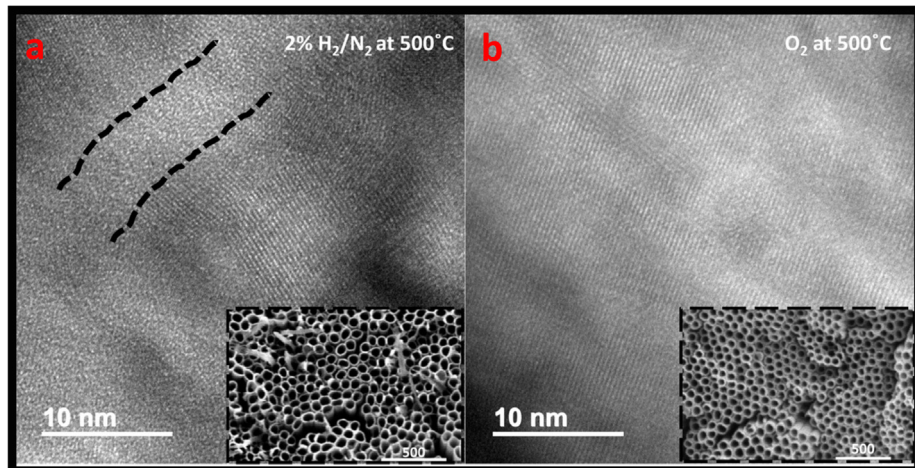


**Fig. 1.** High resolution images of 2% $\text{H}_2$ - $\text{N}_2$ -NTs and  $\text{O}_2$ -NTs **a**. The HRTEM image of the 2% $\text{H}_2$ - $\text{N}_2$ -NTs showing disordered structure between the black dashed lines surrounded by lattice fringes. The inset shows the top view SEM image of the 2% $\text{H}_2$ - $\text{N}_2$ -NTs. **b**. HRTEM image of  $\text{O}_2$ -NTs showing completely crystalline structures with lattice fringes. The inset shows the top view SEM image of the  $\text{O}_2$ -NTs.

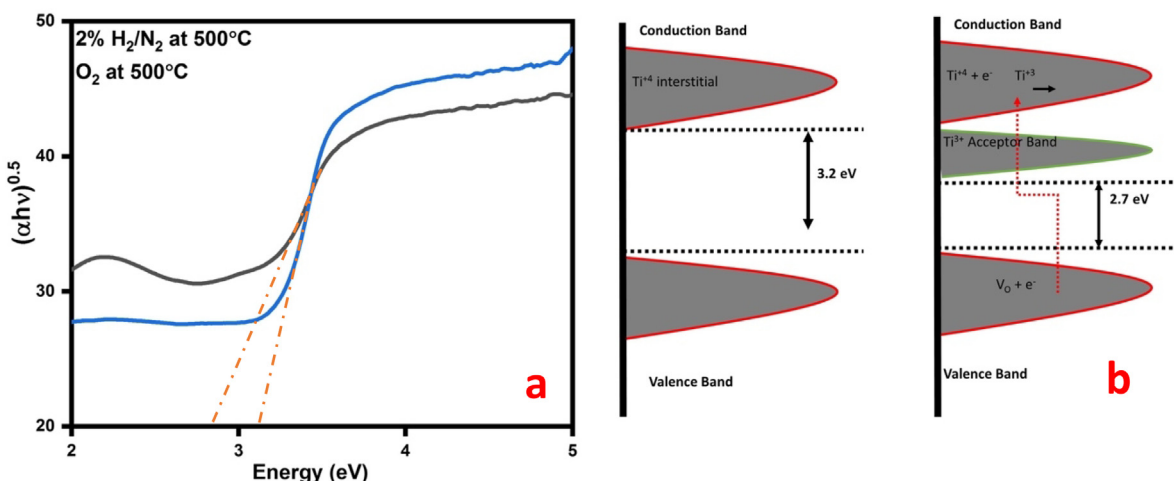


**Fig. 2.** Effects of annealing on optical bandgap **a**. The optical bandgaps extrapolated from Tauc plots for the 2% $\text{H}_2$ - $\text{N}_2$ -NTs and  $\text{O}_2$ -NTs. The 2% $\text{H}_2$ - $\text{N}_2$ -NTs showed smaller optical band and greater absorption in visible light range. **b**. Schematic representing the bandgap narrowing the 2% $\text{H}_2$ - $\text{N}_2$ -NTs from initial 3.2 eV bandgap amorphous nanotubes to formation of acceptor bands below the conduction band under  $\text{H}_2$ - $\text{N}_2$  annealing and causing narrowing of bandgap.

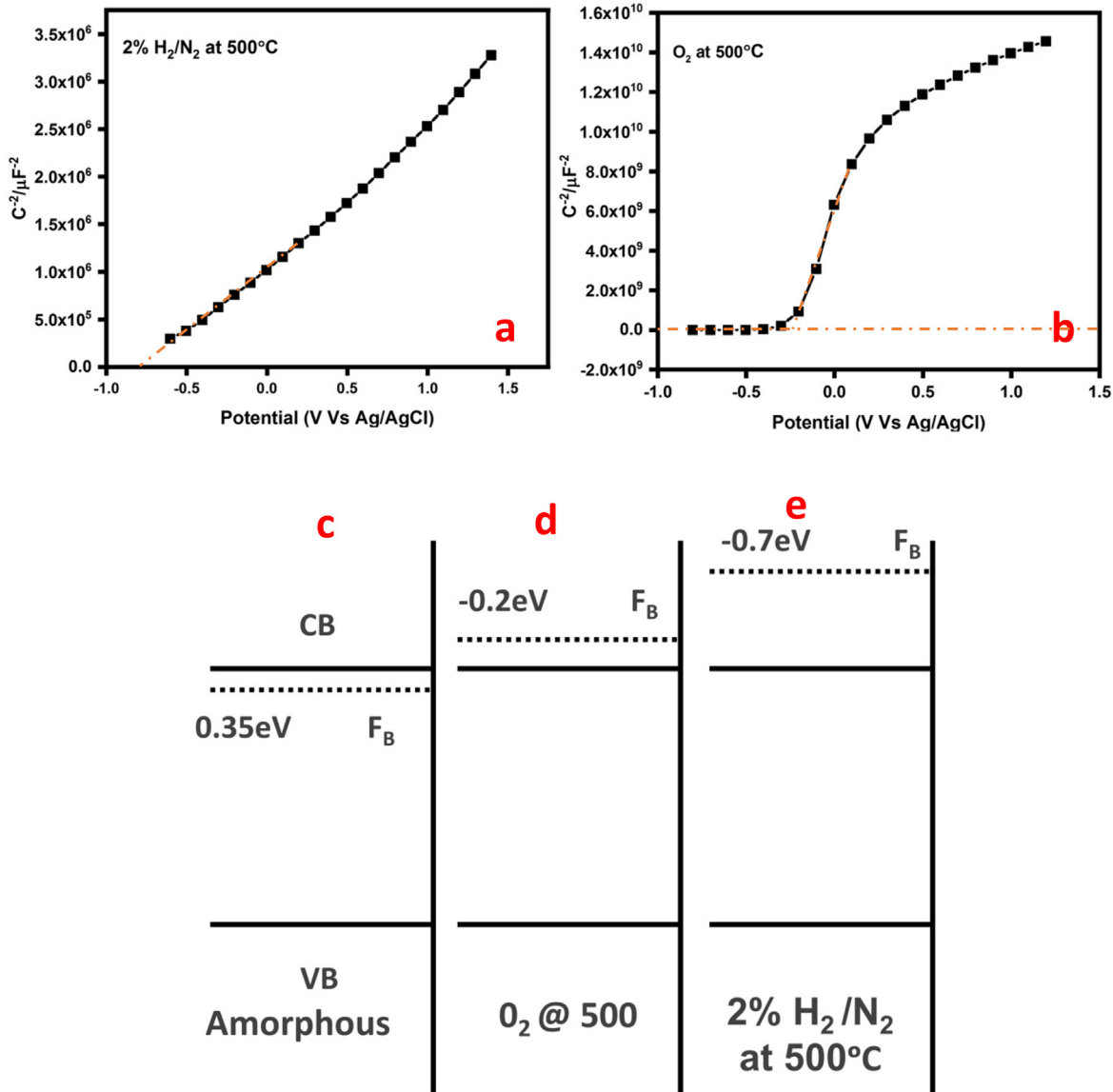


**Fig. 3.** Electrochemical characterization of  $\text{O}_2$ -NTs and 2%  $\text{H}_2/\text{N}_2$ -NTs *a. b.* The Mott Schottky plot of the 2%  $\text{H}_2/\text{N}_2$ -NTs and  $\text{O}_2$ -NTs showing increase in capacitance with potential shifts. *c. d. e.* Schematic illustrating flat band potentials shifts from the amorphous NTs to the  $\text{O}_2$ -NTs and 2%  $\text{H}_2/\text{N}_2$ -NTs with highest negative potential shifts for 2%  $\text{H}_2/\text{N}_2$ -NTs.

anatase to rutile phase transformation is due to the growth of anatase crystallite  $> 20$  nm, which makes the anatase crystallite thermodynamically unstable, leading to the transformation to the stable rutile phase. The formation of a mixed phase anatase–rutile NTs is a function of the anatase crystallite size, as the particle size determines the phase stability for nanocrystalline materials [11]. The optical band structure for  $\text{O}_2$ -NTs did not show visible light absorption (Fig. 2(a)) and the bandgap energy was around 3.2 eV.

The electrochemical response of 2%  $\text{H}_2/\text{N}_2$ -NTs and  $\text{O}_2$ -NTs under an anodic bias was analyzed using electrochemical impedance. This information was used to create Mott Schottky plots ( $C^{-2}$  vs Potential). The Mott Schottky plots were used to determine the shift in the flat band potential ( $E_{fb}$ ) (Fig. 3), where  $E_{fb}$  is determined by extrapolation of linear dependence to  $C^{-2} = 0$  [12].

The 2%  $\text{H}_2/\text{N}_2$ -NTs showed more negative  $E_{fb}$  around  $-0.7$  eV compared to the  $\text{O}_2$ -NTs with  $E_{fb}$  around  $-0.2$  eV (Fig. 3 (d-e)). The defect laden disordered surface of 2%  $\text{H}_2/\text{N}_2$ -NTs suppress the recombination of charge carriers resulting in more negative  $E_{fb}$ .

The negative  $E_{fb}$ , while establishing a thermodynamic equilibrium with the redox potential, makes the 2%  $\text{H}_2/\text{N}_2$ -NTs n-type doped tubes [12]. The large negative  $E_{fb}$  allows more electron transfer at the interface forming a space charge layer with positive charge on the NTs side and negative charge on the electrolyte side of the interface [13]. The 2%  $\text{H}_2/\text{N}_2$ -NTs have defect laden disorder surface and more negative  $E_{fb}$  providing trapping sites for the charge carriers, restricting their recombination upon excitation and allowing much better electron transfer.

## 5. Conclusion:

This study compares the electrochemical behavior of mixed phase anatase–rutile NTs with anatase NTs having a defect laden disordered surface layer. The chemical interaction of the NTs with 2%  $\text{H}_2/\text{N}_2$  results in an oxygen deficient crystal structure at the surface of the NT. This distorted lattice structure contains defects which leads to shallow donor states, altering the bandgap and

distort lattice structure to produce disordered surface layer. This defect laden disordered surface layer becomes the suppression sites for charge recombination leading to more negative flat band potential and increased electrochemical response in 2%H<sub>2</sub>/N<sub>2</sub>-NTs. Conclusively, the NTs with anatase having a defect laden structure results in better electrochemical properties than NTs with anatase-rutile crystal structure. These enhanced electrochemical properties are important when designing the nanomaterial for electrochemical applications such as VOC detection, photocatalytic and/or electrocatalytic degradation of water and airborne pathogens.

#### CRediT authorship contribution statement

**Hamad Malik:** Conceptualization, Methodology, Investigation, Resources, Writing - original draft, Validation. **Kai Barrera:** Investigation, Validation. **Swomitra Mohanty:** Writing - review & editing. **Krista Carlson:** Supervision, Conceptualization, Methodology, Writing - review & editing.

#### Declaration of Competing Interest

The authors declare that they have no known competing financial interests or personal relationships that could have appeared to influence the work reported in this paper.

#### Acknowledgement

This study was supported by NSF (NSF # 1706283), the Roger and Dawn Crus Center, and through the United States Agency for International Development (USAID).

#### Appendix A. Supplementary data

Supplementary data to this article can be found online at <https://doi.org/10.1016/j.matlet.2020.127956>.

#### References

- [1] M. Pelaez, N.T. Nolan, S.C. Pillai, M.K. Seery, P. Falaras, A.G. Kontos, P.S.M. Dunlop, J.W.J. Hamilton, J.A. Byrne, K. O'Shea, M.H. Entezari, D.D. Dionysiou, A review on the visible light active titanium dioxide photocatalysts for environmental applications, *Appl. Catal. B Environ.* 125 (2012) 331–349, <https://doi.org/10.1016/j.apcatb.2012.05.036>.
- [2] P. Roy, S. Berger, P. Schmuki, TiO<sub>2</sub>nanotubes: Synthesis and applications, *Angew. Chemie - Int. Ed.* 50 (2011) 2904–2939, <https://doi.org/10.1002/anie.201001374>.
- [3] X. Chen, L. Liu, P.Y. Yu, S.S. Mao, X. Chen, L. Liu, P.Y. Yu, S.S. Mao, Increasing Solar Absorption for Photocatalysis with Black Hydrogenated Titanium Dioxide Nanocrystals, 331 (2017) 746–750.
- [4] M.G. Beeman, U.C. Nze, H.J. Sant, H. Malik, S. Mohanty, B.K. Gale, K. Carlson, Electrochemical detection of E. Coli O157:H7 in water after electrocatalytic and ultraviolet treatments using a polyguanine-labeled secondary bead sensor, *Sensors (Switzerland)* 18 (2018), <https://doi.org/10.3390/s18051497>.
- [5] K. Carlson, C. Elliott, S. Walker, M. Misra, S. Mohanty, An Effective, Point-of-Use Water Disinfection Device Using Immobilized Black TiO<sub>2</sub> Nanotubes as an Electrocatalyst, *J. Electrochem. Soc.* 163 (2016) H395–H401, <https://doi.org/10.1149/2.0651606jes>.
- [6] H. Liu, H.T. Ma, X.Z. Li, W.Z. Li, M. Wu, X.H. Bao, The enhancement of TiO<sub>2</sub> photocatalytic activity by hydrogen thermal treatment, *Chemosphere* 50 (2003) 39–46, [https://doi.org/10.1016/S0045-6535\(02\)00486-1](https://doi.org/10.1016/S0045-6535(02)00486-1).
- [7] G.H. Lee, J.-M. Zuo, Growth and Phase Transformation of Nanometer-Sized Titanium Oxide Powders Produced by the Precipitation Method, *J. Am. Ceram. Soc.* 79 (2004) 473–479, <https://doi.org/10.1111/j.1551-2916.2004.00473.x>.
- [8] R.S. Hyam, J. Lee, E. Cho, J. Khim, H. Lee, Effect of annealing environments on self-organized TiO<sub>2</sub> nanotubes for efficient photocatalytic applications, *J. Nanosci. Nanotechnol.* 12 (2012) 8908–8912, <https://doi.org/10.1166/jnn.2012.6734>.
- [9] F. Amano, M. Nakata, A. Yamamoto, T. Tanaka, Effect of Ti<sup>3+</sup> Ions and Conduction Band Electrons on Photocatalytic and Photoelectrochemical Activity of Rutile Titania for Water Oxidation, *J. Phys. Chem. C* 120 (2016) 6467–6474, <https://doi.org/10.1021/acs.jpcc.6b01481>.
- [10] H. Malik, S. Sarkar, S. Mohanty, K. Carlson, Modelling and Synthesis of Magnéli Phases in Ordered titanium oxide nanotubes with preserved morphology, *Sci. Rep.* in press (2020).
- [11] H. Zhang, J.F. Banfield, Understanding polymorphic phase transformation behavior during growth of nanocrystalline aggregates: Insights from TiO<sub>2</sub>, *J. Phys. Chem. B* 104 (2000) 3481–3487, <https://doi.org/10.1021/jp000499j>.
- [12] A.W. Bott, Electrochemistry of Semiconductors, *Sol. Energy.* 8 (1998) 136, [https://doi.org/10.1016/0038-092X\(64\)90079-9](https://doi.org/10.1016/0038-092X(64)90079-9).
- [13] R. Beranek, (Photo)electrochemical methods for the determination of the band edge positions of TiO<sub>2</sub>-based nanomaterials, *Adv. Phys. Chem.* 2011 (2011) 80–83, <https://doi.org/10.1155/2011/786759>.